Iontophoresis-mediated direct delivery of nucleic acid therapeutics, without use of carriers, to internal organs via non-blood circulatory pathways

Mahadi Hasan,[1, #] Tatsuya Fukuta,[1, 2, #] Shinya Inoue[1], Hinako Mori,[1] Mayuko Kagawa,[1] Kentaro Kogure[1, *]

[1]*Department of Pharmaceutical Health Chemistry, Graduate School of Biomedical Sciences, Tokushima University, Shomachi 1, Tokushima 770-8505, Japan*

[2]*Department of Physical Pharmaceutics, School of Pharmaceutical Sciences, Wakayama Medical University, 25-1 Shichiban-cho, Wakayama, 640-8156, Japan*

[*]Correspondence author: Kentaro Kogure

TEL: +81-88-633-7248 FAX: +81-88-633-9572

Email: kogure@tokushima-u.ac.jp

Department of Pharmaceutical Health Chemistry, Graduate School of Biomedical Sciences, Tokushima University, Shomachi 1, Tokushima 770-8505, Japan

[#]These authors contributed equally to this work

Abstract

Nanoparticle drug carriers have been employed to achieve systemic delivery of nucleic acid therapeutics, including small interfering RNA (siRNA); however, non-specific distribution and immune-related events often cause undesired adverse effects. Thus, there is a need for a new technology capable of specifically delivering nucleic acid therapeutics to desired sites. We demonstrated the utility of iontophoresis (IP) using weak electric current (0.3-0.5 mA/cm^2) as a local drug delivery technology. Our previous studies revealed that IP allows for transdermal permeation of nucleic acid therapeutics via induction of intercellular junction cleavage initiated by Ca^{2+} influx-mediated cellular signaling activation, and subsequent cytoplasmic delivery through a unique endocytosis process in both skin and other cells. Based on these findings, we hypothesized that IP may enable direct delivery of nucleic acid therapeutics to internal organs through non-blood circulatory pathways without the use of delivery carriers. Permeation of fluorescent-labeled nucleic acids administered via IP applied to the surface of the liver and pancreas was observed in both organs, but not with topical application. IP-mediated local delivery of siRNA into the liver and pancreas significantly suppressed target mRNA expression in each organ. Moreover, IP administration of therapeutic siRNA against the molecules responsible for liver steatosis and fibrosis significantly inhibited lipid accumulation and fibrotic hepatic damage in individual model mice. These findings suggest that IP may be a useful technology to directly deliver nucleic acid therapeutics to internal organs without use of drug delivery carriers via non-blood circulatory pathways.

Keywords

Drug delivery; Iontophoresis; Nucleic acid therapeutics; siRNA; Liver diseases

1. Introduction

Therapeutic drugs can be administered by various routes, such as injection with needles (i.e., intravenous, subcutaneous, intraperitoneal, intramuscular), as well as by oral, transdermal, and transmucosal routes [1]. Oral delivery is widely used for small molecule drugs due to its non-invasiveness and relatively high patient adherence. On the other hand, macromolecular drugs, including proteins, antibodies, and nucleic acids are generally administered subcutaneously or injected into the bloodstream [2]. Systemic delivery of nucleic acid therapeutics, including small-interfering RNA (siRNA), to target organ cells has also been investigated using nanoparticle drug carriers [3, 4]. A recent clinical achievement came with the approval of the lipid nanoparticle patisiran (ONPATTRO^{TM}) for the treatment of hereditary transthyretin amyloidosis, which delivers siRNA that interferes with the production of abnormal transthyretin to liver [5]. In addition, many research efforts have focused on the use of nanoparticle drug delivery systems (DDS) to systemically deliver siRNA and other drugs for cancer therapy [6]. Although nanoparticles are often considered as ideal drug delivery carriers, their non-specific distribution and limited targeting to desired sites (except for liver and spleen) remain challenging and can cause adverse side effects [7]. Surface modification of nanoparticles with polyethylene glycol (PEG) is generally performed to extend circulation time; however, immune reactions against PEG have been reported, raising concerns about the risk of immune-related adverse events [8]. Hence, there is an unmet need to develop a new technology that is capable of delivering macromolecular drugs, especially nucleic acid therapeutics (e.g., siRNA), to specific sites.

To that end, we focused on a transdermal delivery technology iontophoresis (IP) for local drug delivery. IP can noninvasively promote permeation of charged molecules through the skin by application of weak electric current (WEC; 0.3-0.5 mA/cm^2) onto the skin surface [9]. The reason why the current of 0.3-0.5 mA/cm^2 was used for IP would be based on the previous in vivo investigations using animals. The current above 0.5 mA/cm^2 would cause skin damage, such as inflammation and burns, although the currents below 0.3 mA/cm^2 are too weak to induce the

transdermal penetration of drug. IP has conventionally been employed for charged small molecule compounds with relatively high hydrophobicity. On the other hand, we previously reported successful intradermal delivery of charged nanoparticles [10], antibodies [11], and nucleic acid therapeutics [12, 13], and demonstrated the abilities of the delivered agents to carry out their respective biological functions *in vivo*. In particular, IP administration of siRNA showed knockdown of target mRNA in the skin of atopic dermatitis model rats [13].

Although the underlying mechanism of IP-mediated permeation of small molecule drugs had been thought to be via electrorepulsion and electroosmosis [14], we reported additional insights into the mechanism for permeation of macromolecular drugs, which was found to involve activation of certain cellular signaling. Namely, IP treatment induces Ca^{2+} influx into skin cells via a change in membrane potential [15]. Subsequent intracellular signal activation leads to a reduction in the expression of the gap junction protein connexin 43 and depolymerization of the tight junction-associated actin filament, which results in intercellular junction cleavage [16]. Moreover, treatment of cultured cells with WEC has been shown to induce cellular uptake of siRNA via a unique endocytosis, in which endosomes are generated that can leak substances having molecular weights < 70,000, resulting in cytoplasmic delivery of siRNA [15, 17]. These cellular events suggest the potential for intradermal delivery of nucleic acid therapeutics via IP. In addition, we demonstrated that these IP-mediated cellular events are induced not only in the skin but also in other cell types as well [16, 18]. Based on these findings, we hypothesized that IP applied to the surface of internal organs may induce intercellular junction cleavable effects to enable cytoplasmic delivery of nucleic acid therapeutics into the cells of internal organs, similar to the previous findings in skin tissue. If IP is able to noninvasively and directly deliver such therapeutics to internal organs, specific delivery to desired sites through non-blood circulatory pathways could be achieved without the use of delivery carriers (e.g., nanoparticles).

In the present study, we investigated whether direct delivery of nucleic acid therapeutics into internal organs can be achieved via IP administration applied to the tissue surface. As liver

exhibits a relatively large surface area compared with other organs, we first selected liver as a target organ. To further demonstrate the applicability of the IP system to other internal organs, we also investigated the IP-mediated direct delivery of nucleic acids to the pancreas. Finally, we evaluated the therapeutic potential of an IP-mediated direct siRNA delivery system for liver diseases.

2. Methods

2.1. Animals

Male Balb/c mice (5 weeks old) and male Wistar rats (8 weeks old) were purchased from Japan SLC, Inc. (Shizuoka, Japan). Male KK-A^y mice (5 weeks old) were purchased from CLEA Japan, Inc (Tokyo, Japan). All animal protocols were evaluated and approved by the Animal and Ethics Review Committee of Tokushima University.

2.2. Biologicals/Chemicals

Rhodamine-labeled anti-GFP siRNA was purchased from Invitrogen Life Technologies (Carlsbad, CA, USA). 6-carboxyfluorescein (FAM)-labeled NF-κB decoy ODN (FAM-ODN) and all primers used in this study were purchased from Eurofins Genomics (Tokyo, Japan). Mouse anti-GAPDH, anti-Pdx-1, anti-resistin, anti-HSP47, and rat anti-GAPDH siRNA were synthesized by Hokkaido System Science Co. Ltd. (Sapporo, Japan). The sequences of FAM-ODN were as follows: 5'-AGTTGAGGGGACTTTCCCAGGC-3' (FAM labeling at the 3' end) and 5'-GCCTGGGAAAGTCCCCTCAACT-3'. Sequence information for all primers and siRNAs are provided in Tables 1 and 2, respectively. RNeasy Plus Mini Kit was purchased from QIAGEN (Valencia, CA, USA). PrimeScript RT Master Mix (Perfect Real Time) and TB GreenTM Premix Ex TaqTM II (Tli RNaseH Plus) were purchased from Takara Bio (Shiga, Japan). Oil Red O, carbon tetrachloride (CCl_4), Mayer's hematoxylin solution, 1% eosin Y solution, and the assay kit to evaluate ALT and AST (Transaminase CII-Test Wako) were purchased from Wako Pure Chemical (Osaka, Japan). Picrosirius red solution was obtained from Scy Tek Laboratories (Utah, USA). Hydroxyproline colorimetric assay kit was obtained from BioVision Inc. (Milpitas, CA. USA). OCT compound, Perma Fluor Aqueous Mounting Medium, and Entellan New® (hydrophobic mounting medium) were obtained from Sakura Finetek (Tokyo, Japan), Thermo Fisher Scientific (Tokyo, Japan), and Merck Millipore (Tokyo, Japan), respectively. An Ag-AgCl electrode was purchased

from 3 M Health Care (Minneapolis, MN, USA). All other reagents used in this study were of the highest grade available commercially.

2.3. Iontophoresis (IP)

IP was performed in mice according to our previous report with some modifications [11]. Briefly, anesthesia was induced in mice by intraperitoneal injection of chloral hydrate (400 mg/kg mouse) dissolved in PBS. Then, the liver/pancreas was opened by a small surgical incision. For administration of FAM-ODN/rhodamine siRNA/siRNA against target mRNA, an Ag-AgCl electrode (0.5 cm^2) containing nonwoven fabric moistened with 10 μg of ODN/siRNA solution (in 50 μL RNase free water) was placed on the upper surface of the liver/pancreas, and an identical Ag-AgCl electrode containing nonwoven fabric moistened with 50 μL of PBS was also placed 0.5 cm away on the liver/ pancreas. The electrode was then connected to the cathode (FAM-ODN/rhodamine siRNA/siRNA) and anode (PBS) of a power supply (TTI ellebeau Inc., model TCCR-3005, Tokyo, Japan), and a constant current of 0.34 mA/cm^2 was applied for 30 min.

2.4. Intrahepatic/intrapancreatic distribution of fluorescent-labeled oligonucleotides

IP of rhodamine-labeled siRNA in liver and IP of FAM-ODN in pancreas were performed as described above. After 3 h of IP, mice were euthanized, and the corresponding organs were harvested and cut into appropriate pieces. Tissues were embedded in OCT compound, followed by snap freezing with dry ice/ethanol and sectioned into 10 μm thick sections using a cryostat (CM3050S; Leica Biosystems, Tokyo, Japan). Sections were then put on the MAS-coated slide glasses, stained with DAPI, and mounted with Perma Fluor Aqueous Mounting Medium. Fluorescence of the stained liver and pancreas sections was observed using a confocal laser scanning microscope (LSM700, Carl Zeiss, Jena, Germany).

2.5. RNA extraction and quantitative RT-PCR

Twenty-four hours after IP of siRNA (10 μg/mouse; anti-GAPDH siRNA for liver and anti-Pdx-1 siRNA for pancreas), mice were anesthetized by isoflurane inhalation and euthanized by cervical dislocation. Immediately after euthanasia, 10-15 mg of liver/pancreatic tissue was collected from the region of liver/pancreas under the negative electrode cathode containing the reservoir of siRNA. Then total RNA was extracted from the collected tissue using a RNeasy Plus Mini kit (QIAGEN, Valencia, CA, USA) according to the manufacturer's instructions. Total RNA concentration and purity were measured with a Nanodrop 8000 (Thermo Scientific, DE, USA). Subsequently, 200 ng of total RNA was reversely transcribed into cDNA where a reverse transcription reaction was performed at 37°C for 15 min with inactivation of reverse transcriptase at 85 °C for 5 min using PrimeScript RT Master Mix (Perfect Real Time, Takara Bio) and a MJ Mini Personal Thermal Cycler (BioRad Laboratories, Hercules, CA). Next, real-time PCR was performed using TB Green Premix Ex Taq II (Tli RNaseH Plus) and a Thermal Cycler Dice Real-Time System III (Takara Bio). For analysis of the mRNA expression levels of GAPDH and Pdx-1, cDNA was denatured at 95 °C for 30 sec, followed by 40 cycles of 95 °C for 5 sec and 60 °C for 30 sec for amplification. β-Actin or GAPDH mRNA was used as an internal control as appropriate. Relative mRNA expression was determined using the 2-ΔΔCT method. For analysis of the levels of resistin and HSP47 mRNA, total RNA isolation and real-time PCR were performed as described above, whereas liver dissection timing was conducted according to the procedure described below.

2.6. Hematoxylin and eosin (HE) staining

Frozen sections of liver and pancreas (10 μm in thickness) prepared as described above were fixed with 4% paraformaldehyde (PFA) for 10 min in a humidified chamber. After washing with PBS, the sections were stained with Mayer's hematoxylin solution for 10 min at room temperature. Stained sections were then washed with distilled water and subsequently restained with 1% eosin Y solution for 1 min at room temperature. The sections were dehydrated with 80–100%

ethanol, cleared with xylene, and mounted with hydrophobic mounting medium (Entellan New®). Thereafter, the sections were observed with a fluorescence phase-contrast microscope (BZ-9000, Keyence, Osaka, Japan).

2.7. Oil Red O staining

To evaluate the suppression of hepatic lipid accumulation in KK-A^{y} mice, anti-resistin siRNA was administered twice per 3 days, and the liver was dissected at 72 h after the second IP administration. The frozen section of liver was then prepared and attached to a glass slide. The sections were fixed with 4% paraformaldehyde for 10 min at room temperature and briefly washed them with water. The fixed sections were then incubated with 18 mg/ml Oil Red O in a 60% (v/v) 2-propanol solution for 20 min at room temperature, and the lipid droplets in sections were observed with a fluorescence phase-contrast microscope (BZ-9000, Keyence, Osaka, Japan). Next, Oil Red O dissolved in the lipid droplets was extracted with 100% 2-propanol, and its relative concentration was determined by measuring absorbance at 540 nm.

2.8. Mouse model of liver fibrosis

The mouse model of liver fibrosis was prepared according to Golder et al. with some modifications [19]. Briefly, a total of 24 mice were randomly assigned into two groups: a healthy group (n=6) and a CCl_4-treated group (n=18). Balb/c mice were 7 weeks of age at the beginning of the induction of the fibrosis. Mice were given 10% CCl_4 diluted in liquid paraffin (2 mL/kg weight) intraperitoneally for 2 consecutive days per week until 7 weeks to induce liver fibrosis. Then, fibrotic mice were randomly subdivided into 3 experimental groups: fibrosis, fibrosis subjected to IP alone, and fibrosis subjected to IP with anti-HSP47 siRNA. Thereafter, two consecutive doses of anti-HSP47 siRNA (10 μg/mouse/time) were administered by IP as described above and mice were sacrificed at 72 h after the second IP dose, and liver tissues were subsequently harvested and processed for analysis.

2.9. Histological analysis of collagen deposition by Picrosirius red staining

The 10-µm frozen liver sections from fibrotic model mice were prepared, and hydrated with distilled water. Sections were covered by Picrosirius red solution followed by incubation for 1 h. After incubation, sections were washed with acetic acid solution and dehydrated with absolute alcohol. Sections were then mounted with hydrophobic mounting medium (Entellan New®) and observed with a fluorescence phase-contrast microscope (BZ-9000, Keyence, Osaka, Japan). After obtaining images of the sections, the image analysis software of the BZ-9000 microscope was used to determine the percentage of collagen deposited within the stained area.

2.10. Hydroxyproline content, and enzymatic activity assays

Hydroxyproline content was quantified according to the manufacturer's instructions. Briefly, 50 µg of liver tissue was homogenized in 500 ul distilled water. Then, 100 µl of concentrated HCl (6N) was added to 100 µL of tissue homogenate in a pressure-tight, teflon capped vial, followed by hydrolysis at 120°C for 3 h. After hydrolysis, the sample was centrifuged at 10000 x g for 3 min and the precipitate was removed. Ten microliters of each hydrolyzed sample were added to a 96-well plate and dried at 60°C. The sediment was then incubated with 100 µl Chloramine T reagent. After incubation for 5 min at room temperature, 100 µl of the DMAB reagent was added to the mixture and incubated for 90 min at 60°C. After cooling at room temperature, the absorbance was measured at 560 nm in a microplate reader (Tecan Group Ltd., Männedorf, Switzerland). In addition, by using blood samples obtained at the same time of liver sample collection, the enzymatic activities of AST and ALT were determined using Transaminase CII-Test Wako according to the manufacturer's instructions.

2.11. Statistical analysis

Statistical differences among more than 3 groups were evaluated by one-way analysis of variance with the Tukey post-hoc test, whereas those between 2 groups were evaluated by Student's t-test. Data are presented as mean ± standard deviation.

3. Results and Discussion

Hepatic tissue exhibits a relatively large surface area compared with other organs, which was suggested to allow for easy placement of two electrodes (anode and cathode) for IP treatment. Thus, we first investigated the potential of IP for direct delivery of nucleic acid therapeutics into internal organs by using the liver as a target organ site. To that end, the skin above the surface of the liver of anesthetized mice was incised to a size where two electrodes could be placed, and nonwoven fabric (0.5 cm^2) moistened with rhodamine-labeled siRNA solution (10 μg as siRNA dose/50 μL) or PBS (50 μL) was placed on the liver at 0.5 cm away. Then, each nonwoven fabric was attached to an Ag-AgCl electrode (cathode: siRNA) with a surface area of 0.5 cm^2, followed by IP treatment with a constant current of 0.34 mA/cm^2 for 30 min. Three hours after 30-min IP, frozen sections of liver were prepared, and rhodamine fluorescence of siRNA was observed by confocal laser scanning microscopy.

While siRNA fluorescence was not detected in the liver following treatment by topical application of rhodamine-siRNA and cathodal IP of PBS, rhodamine fluorescence was observed in the liver tissue following direct IP administration on the liver (Fig. 1A and Supplementary Fig. 1). To evaluate whether siRNA delivered into the liver can exert its functionality, siRNA against glyceraldehyde-3-phosphate dehydrogenase (GAPDH) was next administered into the liver via IP. At 24 h after siRNA administration, RNA from the liver tissue underneath the electrodes was extracted, and GAPDH mRNA expression was assessed. GAPDH mRNA levels were found to be significantly (40%) suppressed by IP administration of anti-GAPDH-siRNA compared with IP treatment alone (Fig 1B). These results demonstrate the successful delivery of siRNA into the liver via IP, which was taken up by liver cells to result in RNA interference (RNAi) effects, consistent with previously reported findings in skin tissue.

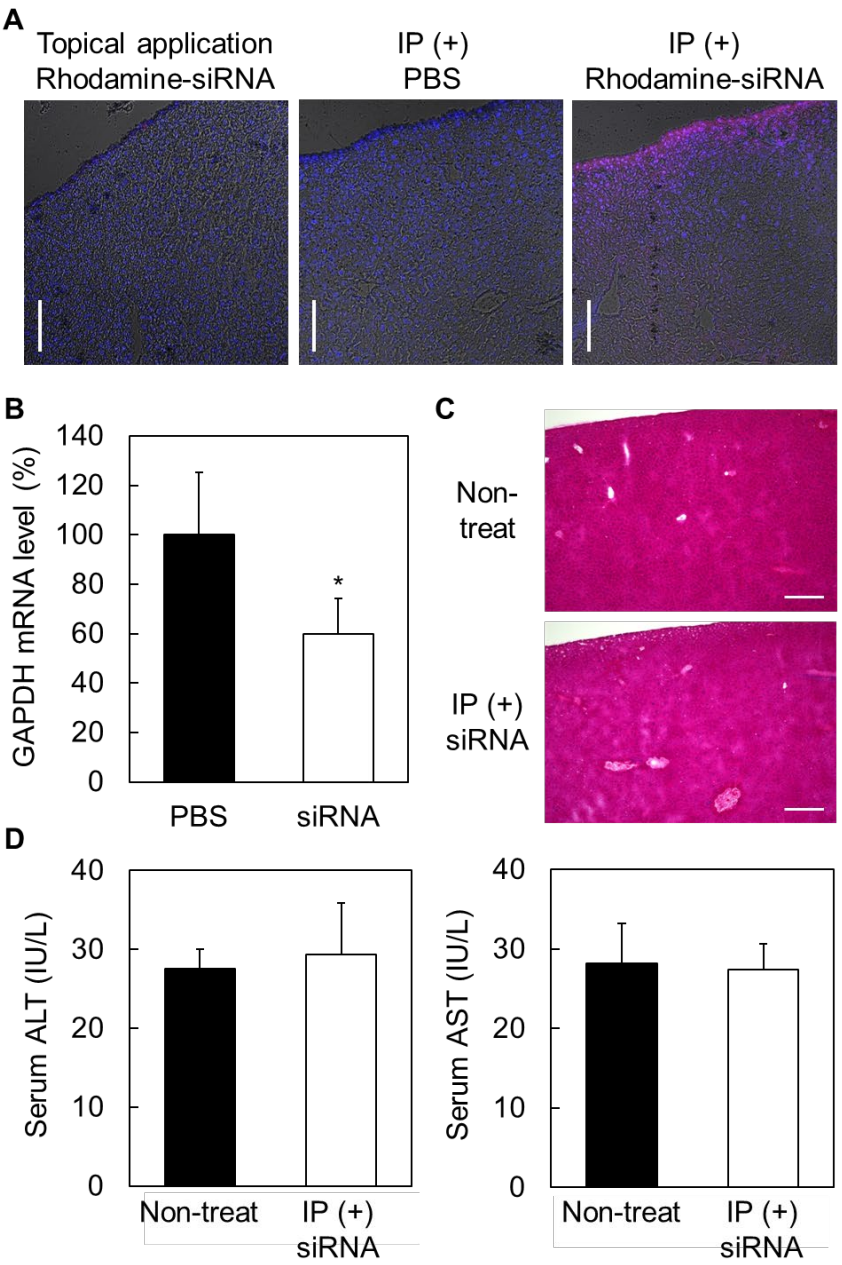

Fig. 1. Delivery of siRNA into the liver by application of IP on the hepatic surface.

(A) Intrahepatic distribution of rhodamine-labeled siRNA at 3 h after IP administration (0.34 mA/cm^2, 30 min). For topical application, nonwoven fabric moistened with fluorescent siRNA solution was attached to an Ag-AgCl electrode and incubated for 30 min without IP treatment (scale bars = 100 μm). (B) Gene silencing effect of GAPDH siRNA (10 μg/mouse) at 24 h after IP administration. (C) Images of HE-stained the liver tissue of non-treated and siRNA-administered groups (scale bars = 200 μm). (D and E) Serum ALT and AST levels were measured at 24 h after IP administration. Data shown are mean ± standard deviation (S.D.) (n=3). * P<0.05.

Previously, it had been reported regarding direct application of nucleic acid onto liver surface by the instillation of plasmid DNA (pDNA) solution [20]. According to the method mentioned in the report, we examined the instillation of anti-GAPDH siRNA solution, of which the concentration was the same as mentioned in the report, onto the surface of liver. The GAPDH mRNA level did not changed significantly, although the average of the mRNA after siRNA instillation was slightly lower than control as shown in the supplemental figure 2. From this result, it was cleared that delivery of siRNA into the liver cells by only instillation on tissue surface. The difference of the result between instillation of pDNA and siRNA would be due to the low delivery efficiency of the instillation method. siRNA should be delivered into many cells to decrease the mRNA level, although expression of luciferase protein even in a few cells would be enough to detect pDNA gene expression. The mechanism of nucleic acid delivery into the cells via the instillation might be due to osmotic lysis of pinocytic vesicles. In the previous report [21], the macromolecules, such as horseradish peroxidase, immunoglobulin G and dextran 70,000, were delivered into cytoplasm via burst of pinocytic vesicles formed in the presence of hypotonic medium. In this additional experiment, since the concentration of siRNA was higher (10 μg/5 μL) than that of IP (10 μg/50 μL), siRNA might be delivered into the liver cells via the osmotic lysis procedure. On the other hand, IP of siRNA showed significant knocking down of GAPDH mRNA (Fig. 1), although the applied amount of siRNA of IP was the same as instillation method. Therefore, the significance of usage of IP in direct transfer from tissue surface is suggested to be the high delivery efficiency into the target cells.

We examined the effect of IP on the tight junction-associated actin filament in the liver using fluorescence-labeled phalloidin to confirm whether the same events as skin reported previously [16] were induced by IP in the liver. The fluorescence indicating filamentous actin in the liver decreased significantly by IP treatment (Supplemental figure 3). The depolymerization of filamentous actin in the liver is the same event in the skin treated with IP reported in previous our publication [16]. Therefore, it was suggested that the mechanism of IP-mediated cytoplasmic

delivery of siRNA in the liver is the same as shown in the skin. However, more detail analysis of the mechanism would be required for the development and application of the direct IP-mediated delivery of nucleic acid therapeutics to internal organ in the future.

We performed a safety evaluation by histological analysis. Results of hematoxylin-eosin (HE) staining showed no apparent liver tissue damage following application of IP on the liver (Fig. 1C). Serum levels of alanine aminotransferase (ALT) and aspartate aminotransferase (AST) were hardly changed between the non-treated group and the group treated with siRNA IP (Fig. 1D), suggesting that IP administration of siRNA hardly induced damage to liver tissue.

To investigate whether such a direct delivery system using IP can be applied to other internal organs, we also performed IP of nucleic acid therapeutics on the pancreas. Cathodal IP of 6-carboxyfluorescein (FAM)-labeled oligodeoxynucleotide (FAM-ODN) was performed on the surface of murine pancreas (0.34 mA/cm^2, 30 min), and frozen sections of pancreas were prepared 3 h after IP. Similar to the results observed in the liver, FAM fluorescence was detected only on the surface of the pancreas following topical application, whereas permeation of FAM-ODN into pancreatic tissue was observed following direct application of IP on the pancreas (Fig. 2A). By using siRNA against pancreatic and duodenal homeobox factor-1 (Pdx-1), a pancreatic specific gene, the knockdown effect of IP-delivered siRNA in the pancreas was evaluated. Pdx-1 mRNA expression was significantly (56%) inhibited at 24 h after IP administration of Pdx-1 siRNA on the pancreas (Fig. 2B). Moreover, obvious pancreatic damage was not observed (Fig. 2C). Based on these results, it is suggested that direct delivery of nucleic acid therapeutics via IP is not liver-specific and can be applied to other internal organs including the pancreas.

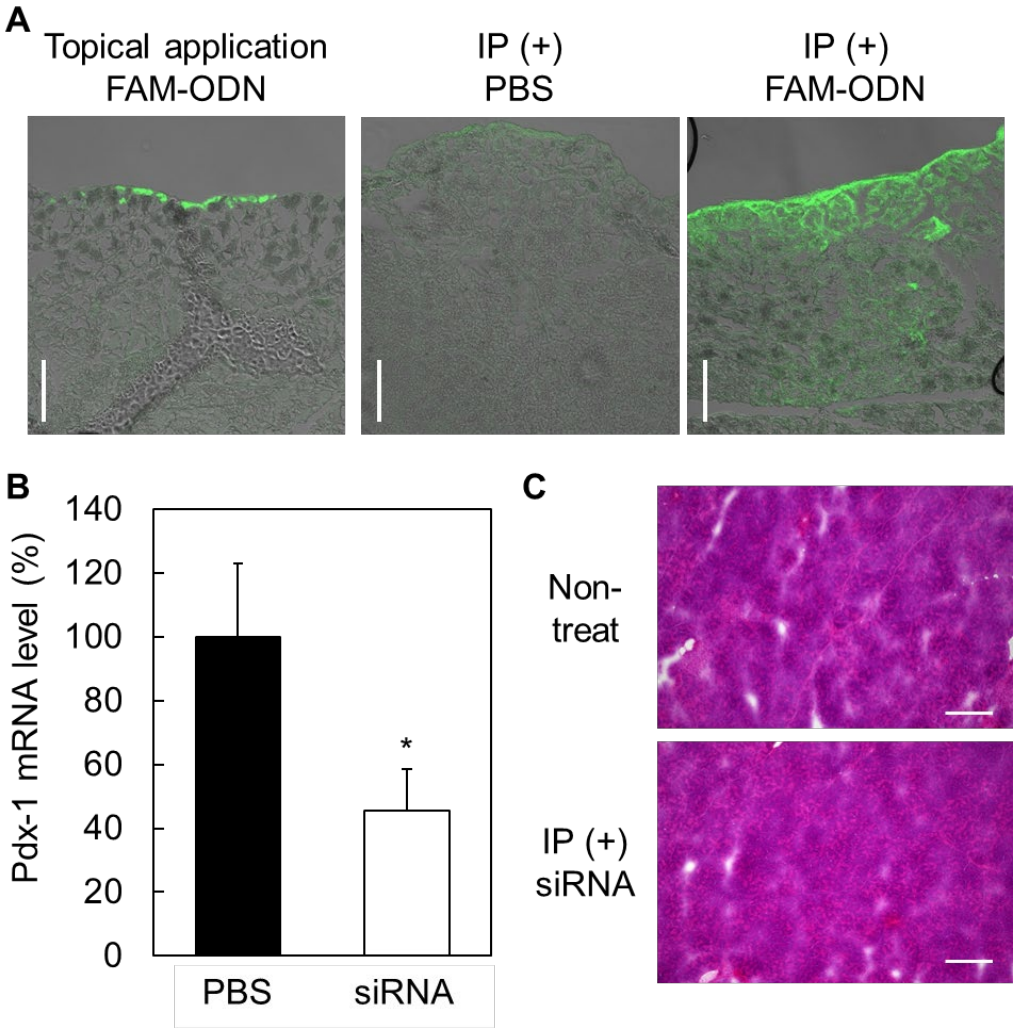

Fig. 2. Direct delivery of nucleic acid therapeutics into the pancreas via IP.
(A) Distribution of FAM-labeled ODN in the pancreas at 3 h after IP administration (0.34 mA/cm^2, 30 min). Scale bars = 100 µm. (B) Knockdown effect of siRNA against Pdx-1 (10 µg/mouse) at 24 h after IP on pancreatic tissue. Data shown are mean ± S.D. (n=4). * P>0.05. (C) Images of HE-stained pancreas tissue of non-treated and siRNA-administered groups (scale bars = 200 µm).

The potential of a direct siRNA delivery system via IP for therapeutic applications was investigated for liver diseases. Non-alcoholic fatty liver disease (NAFLD) is the most common chronic liver disease and ranges from hepatic steatosis to steatohepatitis, fibrosis, and cirrhosis [22]. Although the cause of NAFLD remains to be completely understood, liver steatosis is a prerequisite for subsequent phenomena that bring about liver injury [23]. Thus, suppression of lipid accumulation in the liver may lead to prevention of liver steatosis and subsequent NAFLD. Resistin, an

adipocytokine that is mainly secreted from adipocytes, was reported to be involved in lipid accumulation, and to be abundantly present in liver cells [24, 25]. Indeed, our previous study demonstrated that resistin knockdown by siRNA significantly suppresses lipid accumulation in murine 3T3-L1 cells [18, 24]. Based on these findings, we hypothesized that direct IP delivery of anti-resistin siRNA into liver tissue may affect lipid accumulation in fatty liver, and we tested this hypothesis using obesity model KK-A^y mice. At 24 h after IP administration of anti-resistin siRNA (0.34 mA/cm^2 for 30 min) into the liver of KK-A^y mice, we evaluated the expression level of resistin mRNA in the liver tissue underneath the cathodal electrodes. IP-administered anti-resistin siRNA significantly (53%) suppressed resistin mRNA expression (Fig. 3A). We then administered anti-resistin siRNA twice per 3 days and evaluated the effect of siRNA treatment on liver lipid accumulation at 7 days after the first IP administration. The images of Oil Red O staining showed that the red colors derived from lipid droplets were widely observed in the PBS-administered group (Fig. 3B). However, lipid droplets were markedly reduced in the group receiving two doses of siRNA. The absorbance of Oil Red O dye was also measured after extraction from the liver sections, and showed that anti-resistin siRNA IP partially (but significantly) suppressed hepatic lipid accumulation (Fig. 3C). These results suggest the potential of an IP-mediated direct siRNA delivery system for the treatment of liver steatosis.

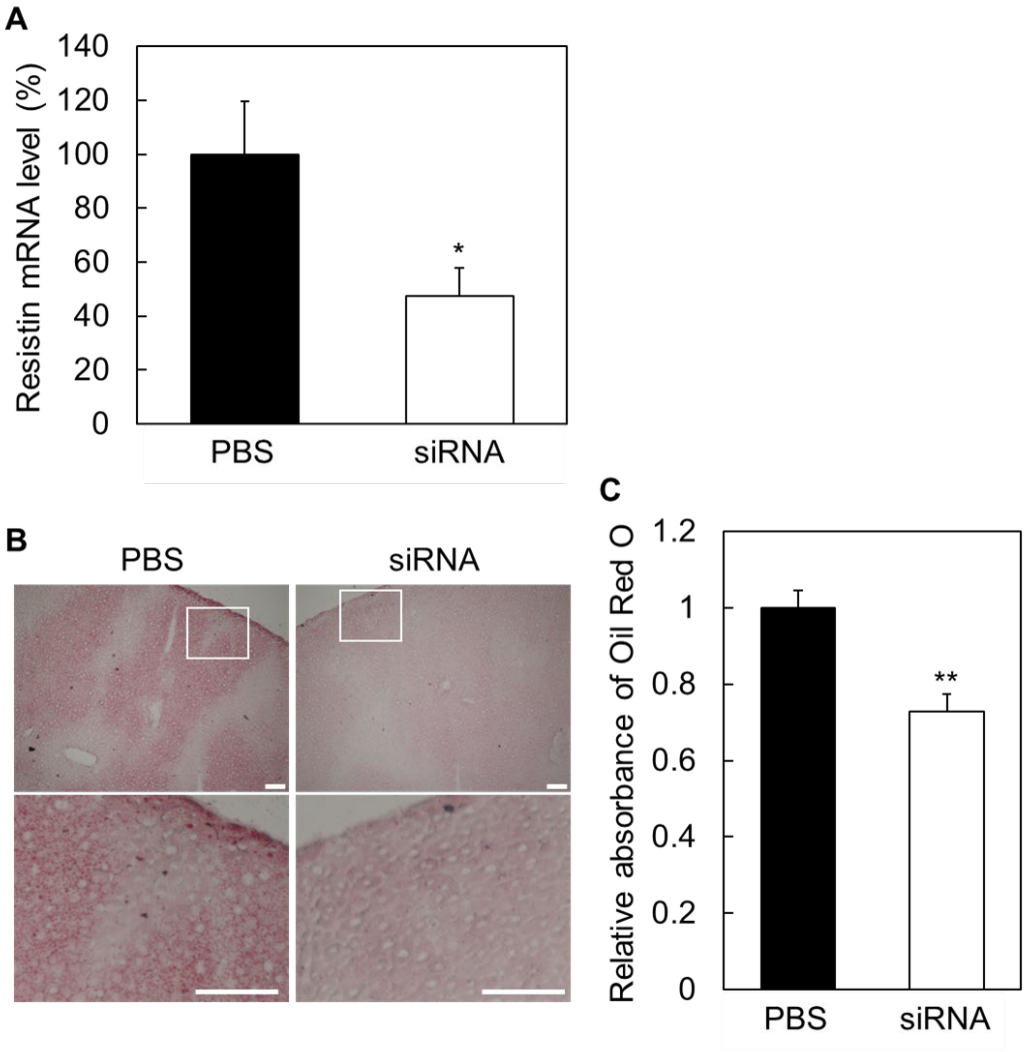

Fig. 3. Suppression of lipid accumulation by anti-resistin siRNA IP administration on fatty liver.
(A) Suppression of resistin mRNA expression after 24 h of IP administration of anti-resistin siRNA (10 μg/mouse/time) into the liver of obesity model KK-A^y mice. To evaluate suppression of hepatic lipid accumulation, siRNA was administered twice per 3 days, and the livers were dissected at 72 h after the second administration. (B) Hepatic images stained with Oil Red O. The lower images show high-magnification of the white squares in the upper images. The red color indicates lipid droplets (scale bars = 100 μm). (C) Lipid accumulation was evaluated by measuring extracted Oil Red O dye from the livers. Data shown are mean ± S.D. (n=3-4). * P<0.05 and ** P<0.01.

To further demonstrate the utility of the IP-mediated direct siRNA delivery system, we next applied the system to the treatment of liver fibrosis, a severe pathology of chronic liver damage. Liver fibrosis is characterized by excessive deposition of extracellular matrix (ECM) proteins,

especially collagen, and hepatic stellate cells play a key role in liver fibrosis [26]. It was previously reported that therapeutic approaches including inhibition of collagen synthesis and activation of matrix metalloproteinases exhibit potential to treat fibrosis; however, side effects resulting from non-specificity are a major problem [27]. On the other hand, collagen secretion from activated hepatic stellate cells was reported to be promoted by a collagen-specific chaperon, namely heat shock protein 47 (HSP47), which is related to translational regulation of procollagen synthesis [28]. As HSP47 is known to be involved in specific association with various collagen types, it is recognized as a promising target for treating liver fibrosis using siRNA [29]. In fact, Sato *et al.* reported the treatment of liver fibrosis using hepatic stellate cell-targeting liposomes encapsulating anti-HSP47 siRNA in dimethylnitrosoamine-treated liver fibrosis model rats [30].

Based on these findings, we investigated the effects of anti-HSP47 siRNA delivered via IP from the surface of fibrotic liver of carbon tetrachloride (CCl_4)-treated liver fibrosis model mice. To induce liver fibrosis, 10% CCl_4 diluted in liquid paraffin was intraperitoneally injected (2 mL/kg weight) twice per week into Balb/c mice [19]. At 7 weeks after the start of fibrosis induction, anti-HSP47 siRNA was administered into the liver by IP twice per 3 days (10 μg/mouse/day), and levels of HSP47 mRNA expression were evaluated at 8 weeks after the start of fibrosis induction. HSP47 mRNA levels were significantly increased by repeated CCl_4 treatment compared with healthy mice (Fig. 4A). Only IP treatment on the fibrotic liver scarcely affected HSP47 mRNA levels, whereas IP administration of anti-HSP47 siRNA significantly inhibited expression. These results suggest that IP-administered siRNA can permeate even into fibrotic liver, and be delivered into the cytoplasm of hepatic cells, resulting in exertion of its RNAi action.

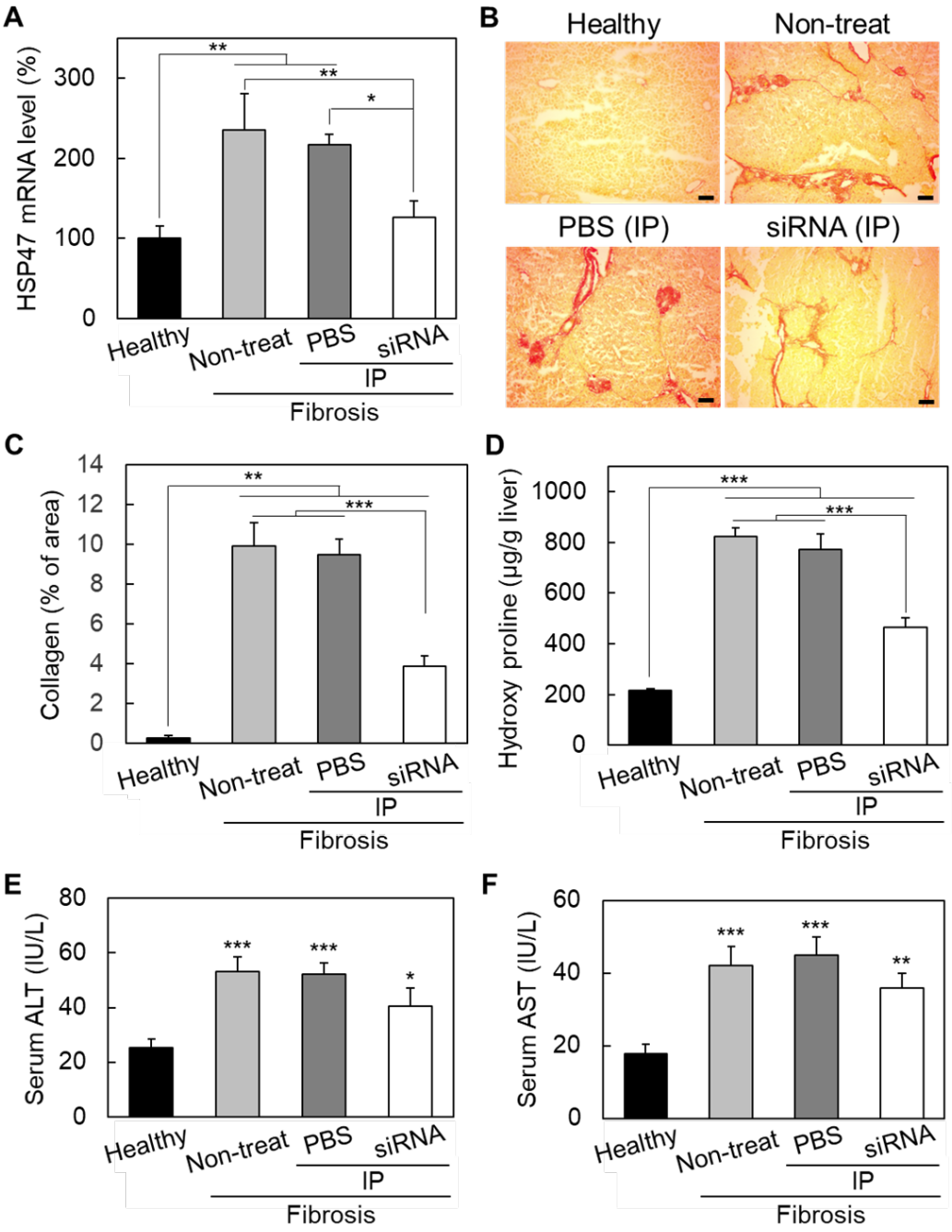

Fig. 4. Amelioration of collagen deposition in fibrotic liver by repeated IP administration of anti-HSP47 siRNA.

(A) Relative expression of HSP47 mRNA in healthy and fibrotic model mice. Anti-HSP47 siRNA was administered (10 μg/mouse/time) twice per 3 days at 7 weeks after the start of fibrosis induction by CCl_4 injection. Livers were dissected at 72 h after the second IP administration. (B) Images of Picrosirius red staining; the red color indicates deposited collagen (scale bars = 100 μm). (C) Collagen deposition (% of area) was quantified using the Image J software. (D) Amount of hydroxyproline in fibrotic liver. (E, F) Evaluation of serum levels of ALT and AST. Data shown are mean ± S.D. (n=3). * P<0.05, ** P<0.01, and *** P<0.001.

Picrosirius red staining showed that collagen accumulation (red region in the images) was clearly induced in the fibrotic liver model mice, and its accumulation was markedly decreased in the group receiving anti-HSP47 siRNA treatment (Fig. 4B). Quantitative results also indicate a suppressive effect of direct anti-HSP47 siRNA delivery on collagen accumulation (Fig. 4C). In addition, the amount of hepatic hydroxyproline, a specific amino acid in collagen, was examined. Results showed that hepatic hydroxyproline content was significantly increased in the IP-only and non-treated groups, compared with healthy mice (Fig. 4D). However, consistent with the collagen staining results, treatment with anti-HSP47 siRNA significantly decreased hydroxyproline levels among the fibrosis model groups. Serum ALT and AST levels were also evaluated, and significant increases were found in the liver fibrosis model (Figs. 4E and F). On the other hand, levels of both enzymes tended to decrease in anti-HSP47 siRNA-treated groups compared with non-treated and PBS-treated groups. These results suggest that the direct delivery of anti-HSP47 siRNA via IP could improve fibrotic damage in the liver by reduction of collagen deposition.

Liver steatosis and fibrosis eventually develop into liver cirrhosis, a severe cause of mortality and morbidity worldwide. Currently, the only effective therapeutic option for liver cirrhosis is liver transplantation; however, transplantation is often limited by availability and suitability of liver grafts [31]. Hence, there is a need for development of new therapies capable of preventing pathological progression of liver steatosis and fibrosis without undesired side effects. The present study demonstrates the usefulness of IP as a local and direct siRNA delivery system to diseased liver. To realize siRNA delivery to the liver via systemic routes, use of drug carriers (e.g., liposomes) has been essential, whereas non-specific distribution and limited targeting to specific organs may cause undesired side effects. However, we demonstrated that IP enables direct delivery of siRNA to hepatic cells through non-blood circulatory pathways without the use of drug carriers. In addition, because IP-mediated delivered siRNA exerted RNAi effects in the liver, cytoplasmic delivery of siRNA could also be achieved in hepatic cells as well as in skin cells.

Drug carriers have been applied to nucleic acid therapeutics, including siRNA, to avoid

enzymatic degradation in the blood stream [32]. Cell-penetrating peptides and cationic materials have also been used frequently to promote cellular uptake and endosomal escape of nucleic acids [32, 33]. Our previous studies demonstrated that WEC employed for IP can induce intercellular junction cleavage in skin tissue, and induce a unique type of endocytosis, in which leaky endosomes are produced that can leak substances with molecular weights <70,000, allowing for cytoplasmic delivery of naked siRNA [15, 17]. The findings of the present study suggest that WEC can also exert an intercellular junction cleavable effect and induce the unique endocytosis of siRNA in liver tissue, similar to previous results observed in skin tissue.

However, the depth of drug penetration by IP would be still limited for the application to large organs, and drugs should be delivered to the deeper region in the human liver. To overcome this point, we are considering the combination of IP with tight junction-opening peptide AT1002, as synergistic effects of weak electricity-mediated intercellular junction cleavage and the tight junction-opening ability of AT1002 may help macromolecule delivery into large organs including human liver. AT1002 is a 6-mer peptide, of which the amino acid sequence is Phe-Cys-Ile-Gly-Arg-Leu, derived from Zonula occuluta toxin, which can reversibly open tight junctions [34]. Recently, we succeeded in the effective delivery of fluorescence labeled NF-κB decoy oligonucleotide (M.W. 13,200) into thickened pathological skin in psoriasis via iontophoresis combined with AT1002 [35]. Therefore, it is expected that macromolecules such as siRNA might be delivered to deeper region even in the human liver by combination of iontophoresis and AT1002 in the future.

In the present study, we also succeeded in IP-mediated direct delivery of siRNA into the pancreas, suggesting that this IP delivery technology could also have applications for treatment of pancreatic diseases. In particular, intractable pancreatic cancer is a candidate disease for use of this type of a delivery technology. As abundant stromal tissues are present in pancreatic cancer tissue, accumulation of therapeutic agents (e.g., small molecule anti-cancer drugs, siRNA) into cancer cells is severely hampered even when using nanoparticle DDS [36]. If IP applied to the surface of the pancreatic cancer can overcome barriers, such as abundant stromal cells, efficient delivery of siRNA

into pancreatic cancer cells may be realized without use of nanoparticles. Thus, application of the IP-mediated direct delivery system for pancreatic cancer therapy would be interesting to investigate in future studies.

Considering clinical applications of the IP-mediated direct siRNA delivery system, one of the obstacles is to low-invasively perform IP treatment on the surface of target tissues, similar to treatment performed on the skin. In this study, we performed IP on internal organs after an abdominal incision sufficient to attach Ag-AgCl electrodes to the organs. However, application of laparoscopic surgery has steadily increased in recent years, which allows for a minimally invasive surgical approach without incision into the abdominal area [37]. Laparoscopic surgery has been demonstrated to be safe and effective for surgery of certain internal organs including the liver and pancreas [37, 38], and various instruments for such surgeries have been developed, including ultrasound transducers and robotic surgical systems [39, 40]. Development of a combined technology comprised of an IP system and laparoscopic surgical devices may lead to a minimally invasive application of IP for internal organs. Also, the combined technology for direct delivery of nucleic acid therapeutics may offer the potential to realize local, minimally invasive, and efficient delivery to desired organs without requiring the use of drug carriers.

4. Conclusions

In conclusion, we succeeded in local and direct delivery of nucleic acid therapeutics into the liver and pancreas by application of IP onto the organs. The siRNA delivered into the organs was found to significantly suppress target mRNA expression. In addition, direct delivery of siRNA against resistin, an adipocytokine involved in lipid accumulation, could decrease lipid droplets in the liver of obesity model KK-A^y mice. Moreover, in CCl_4-induced liver fibrosis model mice, IP-mediated direct delivery of anti-HSP47 siRNA into fibrotic liver was found to suppress HSP47 mRNA in hepatic cells and improve fibrotic damage by reducing collagen deposition. Taken together,

these results suggest that IP is a useful technology to directly deliver nucleic acid therapeutics to internal organs without the use of drug delivery carriers via non-blood circulatory pathways. This is the first report of the application of IP, a transdermal drug delivery technology, to directly deliver drugs to internal organs, as well as therapeutic application of the system for liver diseases.

Acknowledgments

This research was supported by a Grant-in-Aid for Scientific Research from the Japan Society for the Promotion of Science (JSPS, No. 17H03976, 18F18097, 21H03797), and by research grants from The Tokyo Biochemical Research Foundation, Takahashi Industrial and Economic Research Foundation, The Canon Foundation, and The Japanese Foundation for Research and Promotion of Endoscopy. This work was also supported by the Research Program for the Development of Intelligent Tokushima Artificial Exosome (iTEX) from Tokushima University.

Declaration of interest statement

The authors declare no competing financial interests.

References

[1] A.C. Anselmo, Y. Gokarn, S. Mitragotri, Non-invasive delivery strategies for biologics, Nat Rev Drug Discov, 18 (2019) 19-40.

[2] A.M. Vargason, A.C. Anselmo, S. Mitragotri, The evolution of commercial drug delivery technologies, Nat Biomed Eng, (2021).

[3] S. Yonezawa, H. Koide, T. Asai, Recent advances in siRNA delivery mediated by lipid-based nanoparticles, Adv Drug Deliv Rev, 154-155 (2020) 64-78.

[4] D.W. Bartlett, H. Su, I.J. Hildebrandt, W.A. Weber, M.E. Davis, Impact of tumor-specific

targeting on the biodistribution and efficacy of siRNA nanoparticles measured by multimodality in vivo imaging, Proc Natl Acad Sci, 104 (2007) 15549-15554.

[5] T. Coelho, D. Adams, A. Silva, P. Lozeron, P.N. Hawkins, T. Mant, J. Perez, J. Chiesa, S. Warrington, E. Tranter, Safety and efficacy of RNAi therapy for transthyretin amyloidosis, N Engl J Med, 369 (2013) 819-829.

[6] A.C. Anselmo, S. Mitragotri, Nanoparticles in the clinic: An update, Bioeng Transl Med, 4 (2019) e10143.

[7] A.C. Anselmo, S. Mitragotri, Cell-mediated delivery of nanoparticles: taking advantage of circulatory cells to target nanoparticles, J Control Release, 190 (2014) 531-541.

[8] X. Wang, T. Ishida, H. Kiwada, Anti-PEG IgM elicited by injection of liposomes is involved in the enhanced blood clearance of a subsequent dose of PEGylated liposomes, J Control Release, 119 (2007) 236-244.

[9] M. Hasan, A. Khatun, T. Fukuta, K. Kogure, Noninvasive transdermal delivery of liposomes by weak electric current, Adv Drug Deliv Rev, 154-155 (2020) 227-235.

[10] K. Kajimoto, M. Yamamoto, M. Watanabe, K. Kigasawa, K. Kanamura, H. Harashima, K. Kogure, Noninvasive and persistent transfollicular drug delivery system using a combination of liposomes and iontophoresis, Int J Pharm, 403 (2011) 57-65.

[11] T. Fukuta, Y. Oshima, K. Michiue, D. Tanaka, K. Kogure, Non-invasive delivery of biological macromolecular drugs into the skin by iontophoresis and its application to psoriasis treatment, J Control Release, 323 (2020) 323-332.

[12] T. Fukuta, D. Tanaka, S. Inoue, K. Michiue, K. Kogure, Overcoming thickened pathological skin in psoriasis via iontophoresis combined with tight junction-opening peptide AT1002 for intradermal delivery of NF-kappaB decoy oligodeoxynucleotide, Int J Pharm, 602 (2021) 120601.

[13] K. Kigasawa, K. Kajimoto, S. Hama, A. Saito, K. Kanamura, K. Kogure, Noninvasive delivery of siRNA into the epidermis by iontophoresis using an atopic dermatitis-like model rat, Int J Pharm, 383 (2010) 157-160.

[14] R.H. Guy, Y.N. Kalia, M.B. Delgado-Charro, V. Merino, A. López, D. Marro, Iontophoresis: electrorepulsion and electroosmosis, J Control Release, 64 (2000) 129-132.

[15] M. Hasan, A. Nishimoto, T. Ohgita, S. Hama, H. Kashida, H. Asanuma, K. Kogure, Faint electric treatment-induced rapid and efficient delivery of extraneous hydrophilic molecules into the cytoplasm, J Control Release, 228 (2016) 20-25.

[16] S. Hama, Y. Kimura, A. Mikami, K. Shiota, M. Toyoda, A. Tamura, Y. Nagasaki, K. Kanamura, K. Kajimoto, K. Kogure, Electric stimulus opens intercellular spaces in skin, J Biol Chem, 289 (2014) 2450-2456.

[17] T. Torao, M. Mimura, Y. Oshima, K. Fujikawa, M. Hasan, T. Shimokawa, N. Yamazaki, H. Ando, T. Ishida, T. Fukuta, T. Tanaka, K. Kogure, Characteristics of unique endocytosis induced by weak current for cytoplasmic drug delivery, Int J Pharm, 576 (2020) 119010.

[18] M. Hasan, N. Tarashima, K. Fujikawa, T. Ohgita, S. Hama, T. Tanaka, H. Saito, N. Minakawa, K. Kogure, The novel functional nucleic acid iRed effectively regulates target genes following cytoplasmic delivery by faint electric treatment, Sci Technol Adv Mater, 17 (2016) 554-562.

[19] M.R. Golder, J. Liu, J.N. Andersen, M.V. Shipitsin, F. Vohidov, H.V.-T. Nguyen, D.C. Ehrlich, S.J. Huh, B. Vangamudi, K.D. Economides, Reduction of liver fibrosis by rationally designed macromolecular telmisartan prodrugs, Nat Biomed Eng, 2 (2018) 822-830.

[20] S. Fumoto, H. Furukawa, J. Nakamura, K. Nishida, Safety of liver surface instillation of plasmid DNA in normal and carbon tetrachloride-induced hepatitis mice. J Pharm Pharmceut Sci 14 (2011) 274-262.

[21] C.Y. Okada & M. Rchsteriner, Introduction of macromolecules into cultured mammalian cells by osmotic lysis of pinocytic vesicles. Cell 29 (1982) 33-41.

[22] J.D. Browning, J.D. Horton, Molecular mediators of hepatic steatosis and liver injury, The J Clin Invest, 114 (2004) 147-152.

[23] C.P. Day, O.F. James, Steatohepatitis: a tale of two “hits”?, Gastroenterology, 114 (1998) 842-845.

[24] Y. Ikeda, H. Tsuchiya, S. Hama, K. Kajimoto, K. Kogure, Resistin affects lipid metabolism

during adipocyte maturation of 3T3-L1 cells, FEBS J, 280 (2013) 5884-5895.

[25] E. Szalowska, M.G. Elferink, A. Hoek, G.M. Groothuis, R.J. Vonk, Resistin is more abundant in liver than adipose tissue and is not up-regulated by lipopolysaccharide, J Clin Endocrinol Metab, 94 (2009) 3051-3057.

[26] T. Higashi, S.L. Friedman, Y. Hoshida, Hepatic stellate cells as key target in liver fibrosis, Adv Drug Deliv Rev, 121 (2017) 27-42.

[27] R. Bataller, D.A. Brenner, Liver fibrosis, J Clin Invest, 115 (2005) 209-218.

[28] J.J. Sauk, T. Smith, K. Norris, L. Ferreira, Hsp47 and the translation-translocation machinery cooperate in the production of alpha 1 (I) chains of type I procollagen, J Biol Chem, 269 (1994) 3941-3946.

[29] Z. Zhao, C.-Y. Lin, K. Cheng, siRNA-and miRNA-based therapeutics for liver fibrosis, Transl Res, 214 (2019) 17-29.

[30] Y. Sato, K. Murase, J. Kato, M. Kobune, T. Sato, Y. Kawano, R. Takimoto, K. Takada, K. Miyanishi, T. Matsunaga, T. Takayama, Y. Niitsu, Resolution of liver cirrhosis using vitamin A-coupled liposomes to deliver siRNA against a collagen-specific chaperone, Nat Biotechnol, 26 (2008) 431-442.

[31] M. Sun, T. Kisseleva, Reversibility of liver fibrosis, Clin Res Hepatol Gastroenterol, 39 Suppl 1 (2015) S60-63.

[32] X. Chen, L.S. Mangala, C. Rodriguez-Aguayo, X. Kong, G. Lopez-Berestein, A.K. Sood, RNA interference-based therapy and its delivery systems, Cancer Metastasis Rev, 37 (2018) 107-124.

[33] T. Endoh, T. Ohtsuki, Cellular siRNA delivery using cell-penetrating peptides modified for endosomal escape, Adv Drug Deliv Rev, 61 (2009) 704-709.

[34] T. Watts, I. Berti, A. Sapone, T. Gerarduzzi, T. Not, R. Zielke, A. Fasano, Role of the intestinal tight junction modulator zonulin in the pathogenesis of type I diabetes in BB diabetic-prone rats. Proc Natl Acad Sci USA 102 (2005) 2916–2921.

[35] T. Fukuta, D. Tanaka, S. Inoue, K. Michiue, K. Kogure, Overcoming thickened pathological skin in psoriasis via iontophoresis combined with tight junction-opening peptide AT1002 for

intradermal delivery of NF-κB decoy oligodeoxynucleotide. Int J Pharm 602 (2021) 120601.

[36] N. Nishiyama, Y. Matsumura, K. Kataoka, Development of polymeric micelles for targeting intractable cancers, Cancer Sci, 107 (2016) 867-874.

[37] R.I. Troisi, F. Pegoraro, M.C. Giglio, G. Rompianesi, G. Berardi, F. Tomassini, G. De Simone, G. Aprea, R. Montalti, G.D. De Palma, Robotic approach to the liver: Open surgery in a closed abdomen or laparoscopic surgery with technical constraints?, Surg Oncol, 33 (2020) 239-248.

[38] B. Edwin, M.A. Sahakyan, M. Abu Hilal, M.G. Besselink, M. Braga, J.M. Fabre, L. Fernandez-Cruz, B. Gayet, S.C. Kim, I.E. Khatkov, E.C.C.S. Group, Laparoscopic surgery for pancreatic neoplasms: the European association for endoscopic surgery clinical consensus conference, Surg Endosc, 31 (2017) 2023-2041.

[39] J.J.B. Lim, A.G. Erdman, A review of mechanism used in laparoscopic surgical instruments, Mech Mach Theory, 38 (2003) 1133-1147.

[40] J. Arata, S. Kogiso, M. Sakaguchi, R. Nakadate, S. Oguri, M. Uemura, C. Byunghyun, T. Akahoshi, T. Ikeda, M. Hashizume, Articulated minimally invasive surgical instrument based on compliant mechanism, Int J Comput Assist Radiol Surg, 10 (2015) 1837-1843.

Figure legends

Fig. 1. Delivery of siRNA into the liver by application of IP on the hepatic surface.

(A) Intrahepatic distribution of rhodamine-labeled siRNA at 3 h after IP administration (0.34 mA/cm^2, 30 min). For topical application, nonwoven fabric moistened with fluorescent siRNA solution was attached to an Ag-AgCl electrode and incubated for 30 min without IP treatment (scale bars = 100 μm). (B) Gene silencing effect of GAPDH siRNA (10 μg/mouse) at 24 h after IP administration. (C) Images of HE-stained the liver tissue of non-treated and siRNA-administered groups (scale bars = 200 μm). (D and E) Serum ALT and AST levels were measured at 24 h after IP administration. Data shown are mean ± standard deviation (S.D.) (n=3). * $P<0.05$.

Fig. 2. Direct delivery of nucleic acid therapeutics into the pancreas via IP.

(A) Distribution of FAM-labeled ODN in the pancreas at 3 h after IP administration (0.34 mA/cm^2, 30 min). Scale bars = 100 μm. (B) Knockdown effect of siRNA against Pdx-1 (10 μg/mouse) at 24 h after IP on pancreatic tissue. Data shown are mean ± S.D. (n=4). * P>0.05. (C) Images of HE-stained pancreas tissue of non-treated and siRNA-administered groups (scale bars = 200 μm).

Fig. 3. Suppression of lipid accumulation by anti-resistin siRNA IP administration on fatty liver.

(A) Suppression of resistin mRNA expression after 24 h of IP administration of anti-resistin siRNA (10 μg/mouse/time) into the liver of obesity model KK-A^y mice. To evaluate suppression of hepatic lipid accumulation, siRNA was administered twice per 3 days, and the livers were dissected at 72 h after the second administration. (B) Hepatic images stained with Oil Red O. The lower images show high-magnification of the white squares in the upper images. The red color indicates lipid droplets (scale bars = 100 μm). (C) Lipid accumulation was evaluated by measuring extracted Oil Red O dye from the livers. Data shown are mean ± S.D. (n=3-4). * P<0.05 and ** P<0.01.

Fig. 4. Amelioration of collagen deposition in fibrotic liver by repeated IP administration of anti-HSP47 siRNA.

(A) Relative expression of HSP47 mRNA in healthy and fibrotic model mice. Anti-HSP47 siRNA was administered (10 μg/mouse/time) twice per 3 days at 7 weeks after the start of fibrosis induction by CCl_4 injection. Livers were dissected at 72 h after the second IP administration. (B) Images of Picrosirius red staining; the red color indicates deposited collagen (scale bars = 100 μm). (C) Collagen deposition (% of area) was quantified using the Image J software. (D) Amount of hydroxyproline in fibrotic liver. (E, F) Evaluation of serum levels of ALT and AST. Data shown are mean ± S.D. (n=3). * P<0.05, ** P<0.01, and *** P<0.001.

Table 1. Primer sequences for RT-PCR.

Gene	Forward (5’ to 3’)	Reverse (5’ to 3’)
GAPDH (mouse)	ACCATCTTCCAGGAGCGAGA	GCATGGACTGTGGTCATGAG
β-actin (mouse)	TGTGATGGTGGGAATGGGTCAG	TTTGATGTCACGCACGATTTCC
Resistin	TCACTTTTCACCTCTGTGGATATGAT	TGCCCCAGGTGGTGTAAA
HSP47	CTGCAGTCCATCAACGAGTGGGC	ATGGCGACAGCCTTCTTCTGC
GAPDH (rat)	CCCCCAATGTATCCGTTGTG	TAGCCCAGGATGCCCTTTAGT
β-actin (rat)	ACTATCGGCAATGAGCGGTTCC	CTGTGTTGGCATAGAGGTCTTTACG

Table 2. siRNA sequences.

Target gene	Sence (5’ to 3’)	Anti-sense (5’ to 3’)
GFP	GCUGACCCUGAAGUUCAUCTT	GAUGAACUUCAGGGUCAGCTT
GAPDH (mouse)	CAAGAGAGGCCCUAUCCCATT	UGGGAUAGGGCCUCUCUUGTT
Resistin	CCAAAUGCAAUAAAGAACAUUGGCU	AGCCAAUGUUCUUUAUUGCAUUUGG
HSP47	CTGCAGTCCATCAACGAGTGGGC	ATGGCGACAGCCTTCTTCTGC
GAPDH (rat)	GGUCGGUGUGAACGGAUUUTT	AAAUCCGUUCACACCGACCTT